

Measurement of the reaction $\pi^+n_1 \rightarrow \pi^+\pi^-p$ at 5.98 and 11.85 GeV/c using a transversely polarized deuteron target

A. de Lesquen, L. van Rossum, M. Svec,* M. Babou,† J. Bystricky, G. Cozzika, T. Dobrowolski, Y. Ducros, M. Fujisaki,‡ A. Gaidot, C. F. Hwang,§ A. Itano,** F. Khantine-Langlois and F. Lehar

Département de Physique des Particules Élémentaires, Centre d'Études Nucléaires de Saclay, Boite Postale No.2, F-91191 Gif-sur-Yvette Cedex, France

(Received 12 October 1984)

In an experiment carried out at the CERN Proton Synchrotron and using the CERN polarized deuteron target, the reaction $\pi^+n_1 \rightarrow \pi^+\pi^-p$ has been measured in the region $-t=0.1-1.0$ (GeV/c)² and $m(\pi^+\pi^-)=0.36-1.04$ GeV at incident momenta of 5.98 and 11.85 GeV/c. We present the m and t dependence of the measured 14 linearly independent spin-density-matrix elements and of the bounds on the moduli squared of the S - and P -wave recoil transversity amplitudes. The results show the presence of “ A_1 ” exchange in the unnatural nucleon-helicity-nonflip amplitudes. The natural “ A_2 ”-exchange amplitudes dominate at large t . In the range $0.2 \leq -t \leq 0.4$ (GeV/c)² the mass dependence shows that the unnatural exchange amplitudes with transversity “down” are generally larger than those with transversity “up.” The opposite is true for the natural exchange. In this range of t and at the ρ^0 mass, the P -wave unnatural amplitudes with both transversities contribute in equal amounts while the production by natural exchange proceeds entirely with transversity up. We observe rapid changes of the moduli within the ρ^0 mass range and variations of the width and the position of the ρ^0 peak in spin-averaged partial-wave cross sections. These structures have not been seen in previous polarization experiments and reveal spin dependence of ρ^0 production. Our bounds cannot exclude an S -wave resonance in the range 700–800 MeV. The results emphasize the need for a better experimental and theoretical understanding of the mass dependence of the production mechanism.

I. INTRODUCTION

In an experiment designed to measure the K^+n charge-exchange reaction on polarized neutrons,¹⁻³ we have studied simultaneously the production of pion pairs by positive pions incident on neutrons polarized transversely to the beam direction. In addition to the five normalized spin-density-matrix elements for production on unpolarized nucleons, this measurement yields six more matrix elements depending on the target polarization component normal to the production plane and three elements depending on the transverse component in the production plane. Average values of the 14 normalized spin-density-matrix elements are measured in small regions of four-momentum transfer squared $-t$ and dipion invariant mass m , covering the region $0.1 \leq -t \leq 1.0$ (GeV/c)² and $0.36 \leq m \leq 1.04$ GeV at laboratory incident momenta 5.98 and 11.85 GeV/c.

Previous measurements of $\pi^+n \rightarrow \pi^+\pi^-p$ were performed on unpolarized targets.^{4,5} The CERN-Munich-Cracow measurement⁶ of $\pi^-p \rightarrow \pi^+\pi^-n$ on polarized proton target at 17.2 GeV/c covered a kinematic region in m and t different from our experiment, as shown in Fig. 1. The main objective of the CERN-Munich-Cracow experiment was to provide data at low $|t| \leq 0.15$ (GeV/c)² where pion exchange dominates, and thus aid in the study of $\pi\pi$ scattering.⁷ Our experiment covers a broader range of mass at larger values of $|t| \geq 0.1$ (GeV/c)². It provides new information about the mass dependence of natural and unnatural exchange amplitudes. Theoretical

understanding of the mass dependence of exchange amplitudes in production processes is still lacking,⁸ and only a few studies have been attempted.⁹ At fixed dipion mass, a Regge model which includes A_1 -exchange amplitudes¹⁰ gives a good description of $\pi^-p \rightarrow \rho^0n$ polarized data at 17.2 GeV/c (Ref. 6).

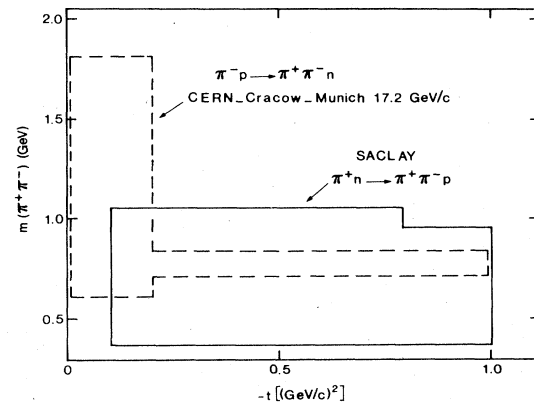


FIG. 1. Region of four-momentum transfer squared and dipion invariant mass for the present experiment. The kinematic region of the published results of the CERN-Munich-Cracow experiment (Ref. 6) is shown for comparison. Unlike the present experiment, the CERN-Munich-Cracow apparatus did not detect the nucleon in the final state. Its acceptance therefore extends to low values of t .

For dipion masses $m < \simeq 1.0$ GeV only two S -wave and six P -wave complex amplitudes dominate. The most convenient choice of amplitudes¹¹ are the recoil transversity amplitudes (RTA). Six linear expressions relate the eight moduli squared of the S - and P -wave RTA to six measured quantities. We use these relations in the present paper to construct bounds on the moduli of the RTA. However, the 14 observables measured in experiments with transversely polarized target are sufficient to determine the S - and P -wave RTA except for the overall phase and for the relative phase between the two groups of four amplitudes each with recoil transversities “up” and “down,” respectively. Two solutions for moduli of amplitudes exist in this amplitude analysis. The ambiguity can be removed and the missing relative phase determined only in experiments measuring also recoil-nucleon polarization.

Preliminary results of our experiment and the associated amplitude analysis were published earlier.¹² In the present paper we outline the kinematics (Sec. II), the experiment (Sec. III), the data analysis (Sec. IV), and discuss the experimental results (Sec. V). An amplitude analysis of $\pi^+n \rightarrow \pi^+\pi^-p$ will be published separately.¹³ Tables with complete numerical results for the spin-density-matrix elements and the corresponding solutions for amplitudes as well as the tests of parity conservation and D -wave contributions are available on request.¹⁴

II. KINEMATICS, OBSERVABLES, AMPLITUDES

The kinematical variables describing the dipion production on a transversely polarized nucleon target at rest are $(s, t, m, \theta, \phi, \psi)$. Here s is the center-of-mass-system energy squared, t is the four-momentum transfer squared, and m is the $(\pi^+\pi^-)$ invariant mass. The angles θ and ϕ describe the direction of the π^+ meson in the $(\pi^+\pi^-)$ rest frame. Our analysis is carried out in both the s -channel

and the t -channel helicity frames of reference for the dipion system. The helicities of the initial and final nucleons are always defined in the s -channel helicity frame.^{10,11} The angle ψ gives the orientation of the production plane with respect to the transverse polarization, as shown in Fig. 2. The effect of Fermi motion of the target neutron in the laboratory system introduces a small correction to the effective neutron polarization. This point is discussed in Sec. III C.

At fixed values of s , t , and m the angular distribution $I(\theta, \phi, \psi)$ for $(\pi^+\pi^-)$ production on polarized nucleons at rest can be expressed in terms of the normalized distribution $W(\theta, \phi, \psi)$

$$I(\theta, \phi, \psi) = W(\theta, \phi, \psi) d^2\sigma / (dt dm), \quad (2.1)$$

where

$$d^2\sigma / (dt dm) = \int I(\theta, \phi, \psi) d\Omega d\psi$$

is the $\pi^+\pi^-$ production cross section. The distribution $W(\theta, \phi, \psi)$ can be written^{10,11} as a sum of four terms

$$W(\theta, \phi, \psi) = W_a(\theta, \phi) + P_T \cos\psi W_b(\theta, \phi) + P_T \sin\psi W_c(\theta, \phi) + P_L W_d(\theta, \phi), \quad (2.2)$$

where P_T (P_L) is the transverse (longitudinal) target-polarization component with respect to the incident momentum (Fig. 2). Parity conservation requires that W_a and W_b (W_c and W_d) are symmetric (antisymmetric) in ϕ . The present experiment does not measure W_d since $P_L \simeq 0$.

Our search for D -wave contribution confirmed that only dipion states $\pi^+\pi^-$ with the total angular momentum $J=0$ (S -wave) and $J=1$ (P wave) contribute to the angular distributions W_a , W_b , and W_c . The normalized distribution can then be written^{10,11} in terms of the $\pi^+\pi^-$ spin-density-matrix elements as

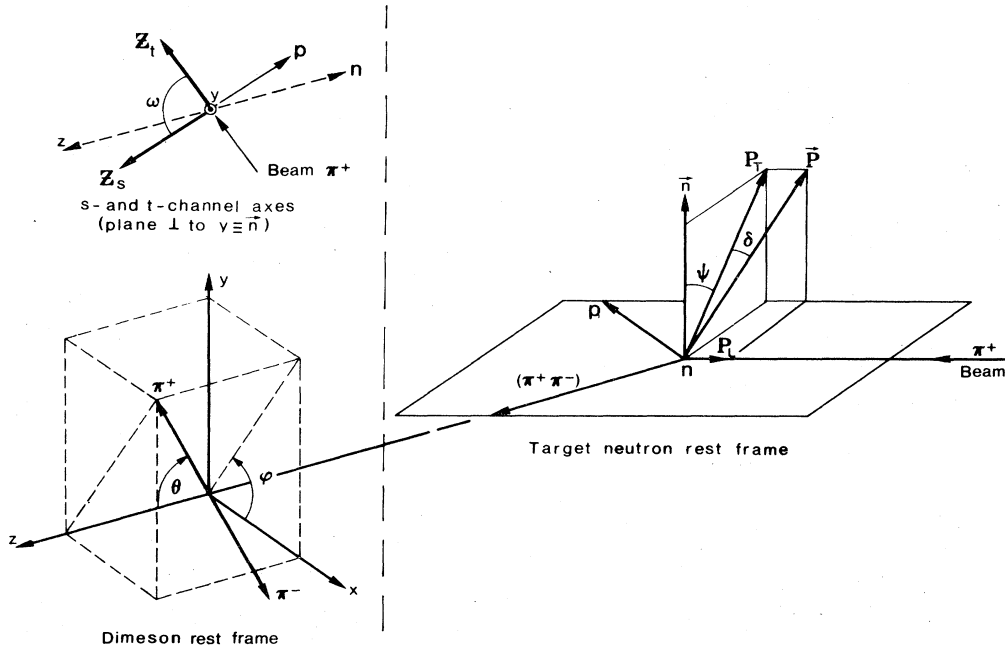


FIG. 2. Definition of the coordinate systems used to describe the target polarization P and the decay of the dipion system.

$$\begin{aligned}
4\pi W(\theta, \phi, \Psi) |_{s,t,m} = & [(\rho_{ss} + \rho_{00} + 2\rho_{11}) + (\rho_{00} - \rho_{1-1})(3 \cos^2\theta - 1) - \rho_{1-1}3 \sin^2\theta \cos 2\phi \\
& - \text{Re}\rho_{10}3\sqrt{2} \sin 2\theta \cos\phi + \text{Re}\rho_{0s}2\sqrt{3} \cos\theta - \text{Re}\rho_{1s}2\sqrt{6} \sin\theta \cos\phi] \\
& + P_T \cos\Psi [(\rho_{ss}^y + \rho_{00}^y + 2\rho_{11}^y) + (\rho_{00}^y - \rho_{1-1}^y)(3 \cos^2\theta - 1) - \rho_{1-1}^y3 \sin^2\theta \cos 2\phi \\
& - \text{Re}\rho_{10}^y3\sqrt{2} \sin 2\theta \cos\phi + \text{Re}\rho_{0s}^y2\sqrt{3} \cos\theta - \text{Re}\rho_{1s}^y2\sqrt{6} \sin\theta \cos\phi] \\
& + P_T \sin\Psi [\text{Im}\rho_{1-1}^x3 \sin^2\theta \sin 2\phi + \text{Im}\rho_{10}^x3\sqrt{2} \sin 2\theta \sin\phi + \text{Im}\rho_{1s}^x2\sqrt{6} \sin\theta \sin\phi] .
\end{aligned} \tag{2.3}$$

The helicity λ of the $\pi^+\pi^-$ system is $\lambda=s$ and $\lambda=-1,0,1$ for S wave and P wave, respectively. There are two relations¹¹ among the matrix elements in (2.3):

$$\rho_{ss} + \rho_{00} + 2\rho_{11} = 1, \tag{2.4a}$$

$$\rho_{ss}^y + \rho_{00}^y + 2\rho_{11}^y = A, \tag{2.4b}$$

where A is the polarized-target asymmetry [see Eq. (4.5)].

For reasons of brevity we shall write the expression (2.3) in a simplified form

$$4\pi W(\theta, \phi, \psi) = 1 + \sum_{i=2}^{15} a_i c_i(\psi) Y_i(\theta, \phi), \tag{2.5}$$

where the coefficients $c_i=1$ for $i=2, \dots, 6$, $c_i=P_T \cos\psi$ for $i=7, \dots, 12$, and $c_i=P_T \sin\psi$ for $i=13, 14, 15$. The parameters a_i , $i=2, \dots, 15$, are the combinations of normalized spin-density-matrix elements in Eq. (2.3) that are to be determined by the experiment.

The reaction $\pi^+n \rightarrow \pi^+\pi^-p$ is described by production amplitudes $H_{\lambda_p, 0\lambda_n}(s, t, m, \theta, \phi)$ where λ_p and λ_n are helicities of the proton and neutron, respectively. The production amplitudes can be expanded into partial-wave amplitudes:

$$H_{\lambda_p, 0\lambda_n} = \sum_{J=0}^{\infty} \sum_{\lambda=-J}^{+J} (2J+1)^{1/2} H_{\lambda\lambda_p, 0\lambda_n}(s, t, m) d_{\lambda 0}^J(\theta) e^{i\lambda\phi}, \tag{2.6}$$

where λ is the helicity of the meson system. The S - and P -wave amplitudes $H_{\lambda\lambda_p, 0\lambda_n}^J$ can be expressed in terms of nucleon helicity amplitudes with definite naturality:

$$\begin{aligned}
H_{0+,0+}^0 &= S_0, & H_{0+,0-}^0 &= S_1, \\
H_{0+,0+}^1 &= L_0, & H_{0+,0-}^1 &= L_1,
\end{aligned} \tag{2.7}$$

$$H_{\pm 1, +0+}^1 = \frac{1}{\sqrt{2}}(N_0 \pm U_0), \quad H_{\pm 1, +0-}^1 = \frac{1}{\sqrt{2}}(N_1 \pm U_1).$$

The amplitudes S_n, L_n, U_n , $n=0,1$, are dominated, at large s , by unnatural exchanges: “ A_1 ” exchange for $n=0$ and “ π ” exchange for $n=1$. The amplitudes $N_n, n=0,1$, are dominated by natural “ A_2 ” exchange. Here $n = |\lambda_n - \lambda_p|$ is the nucleon helicity flip.

The observables obtained in experiments on transversely polarized targets are most simply related to recoil nucleon transversity amplitudes (RTA) which are defined^{10,11} as

$$\begin{aligned}
S &= \frac{1}{\sqrt{2}}(S_0 + iS_1), & \bar{S} &= \frac{1}{\sqrt{2}}(S_0 - iS_1), \\
L &= \frac{1}{\sqrt{2}}(L_0 + iL_1), & \bar{L} &= \frac{1}{\sqrt{2}}(L_0 - iL_1), \\
U &= \frac{1}{\sqrt{2}}(U_0 + iU_1), & \bar{U} &= \frac{1}{\sqrt{2}}(U_0 - iU_1), \\
N &= \frac{1}{\sqrt{2}}(N_0 - iN_1), & \bar{N} &= \frac{1}{\sqrt{2}}(n_0 + iN_1).
\end{aligned} \tag{2.8}$$

The amplitudes S, L, U, N ($\bar{S}, \bar{L}, \bar{U}, \bar{N}$) describe the production of final states with recoil-nucleon spin parallel (anti-parallel) to the normal to the production plane, corresponding to recoil transversity “up” (“down”).

III. THE EXPERIMENT

A. Experimental setup and data acquisition

The experiment was carried out at the CERN Proton Synchrotron. The CERN Polarized Target Group had achieved more than 40% deuteron polarization in deuterated propanediol, thus providing the possibility to study reactions on quasifree polarized neutrons. The apparatus was designed primarily for² $K^+n \uparrow \rightarrow K^0p$ but the trigger logic had been implemented also for $\pi^+n \uparrow \rightarrow \pi^+\pi^-p$ and for several other reactions.³ The $\pi^+\pi^-$ pair was detected in the forward spectrometer, and the proton in one of the recoil arms (Fig. 3). A detailed description of beam, target, detectors, trigger logic, and electronics is given in Ref. 1.

The data acquisition used a PDP 11-45 with 28K memory and standard CAMAC interface. The software based on the RT 11 monitor and the acquisition hardware had been developed and matched for high data acquisition rate. The overall dead time for acquiring the about 200 photomultipliers, 12 ADC's (analog-to-digital converters) and 15000 MWPC (multiwire proportional chamber) wires was 1.3 msec. The sum of the different triggers was about 15 events per burst, with 6 to 8% dead-time losses.

B. Event reconstruction and selection

Forward-emitted pairs of particles of opposite signs were reconstructed from the coordinates in the 12 wire planes of the spectrometer using the principal-components method.¹ The proton trajectory in the recoil spectrometer was reconstructed. The direction of the incident particle was given by the beam hodoscopes. From the χ^2 of the overall fit with the hypothesis $\pi^+n \rightarrow \pi^-p$ it was decided if the event corresponded to the expected reaction. The one constraint fit yielded the four-momentum transfer

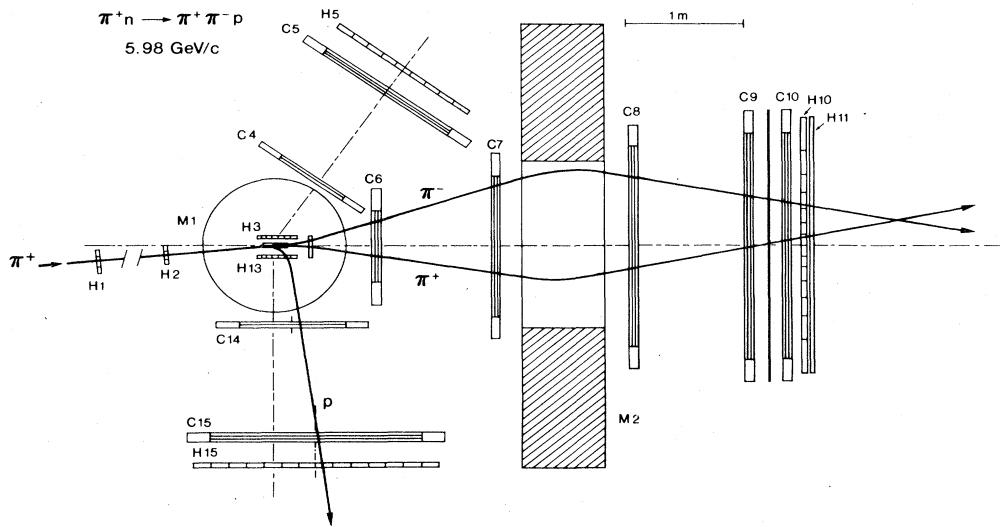


FIG. 3. The layout of the experiment at 5.98 GeV/c. H_1, \dots, H_{15} are triggering hodoscopes; C_1, \dots, C_{15} are multiwire proportional chambers; M_1 and M_2 are the target and spectrometer magnet, respectively.

squared t , the normal to the reaction plane, the invariant dipion mass m and the direction of the π^+ in the dipion rest frame. The target-neutron Fermi momentum \mathbf{p}_F was reconstructed from momentum conservation and the target particle effective mass was calculated requiring that the total energy of the neutron of momentum \mathbf{p}_F plus the energy of the unobservable spectator proton of momentum $-\mathbf{p}_F$ equals the free deuteron mass.¹⁵ The experimental resolution in t and m was approximately $\Delta t = 0.015$ (GeV/c)² and $\Delta m = 0.010$ GeV, respectively. The absolute calibration in m was better than 1%. Event reconstruction, tests of stability for detection and reconstruction efficiencies and consistency checks of different normalization procedures for runs with alternate signs of target polarization have been described in Ref. 1. Special runs with a liquid deuterium target have yielded good agreement between the experimental and the theoretical Fermi momentum distributions, showing that the experiment selects a clean sample of interactions on quasifree neutrons. Reconstruction of events from a liquid hydrogen target without assuming the proton to be at rest has provided a direct measure of the experimental resolution $\Delta p_F \simeq 0.030$ GeV/c.

The event reconstruction and selection resulted in 60 000 events at 5.98 GeV/c incident momentum and 39 000 events at 11.85 GeV/c in the kinematic region of the analysis (Fig. 1). The raw dipion mass distribution shows that $\pi^+n \rightarrow \pi^+\pi^-p$ proceeds predominantly via $\pi^+n \rightarrow \rho^0 p$. Although this does not exclude some contribution from other channels leading to the same final state. The Dalitz plots $m(\pi^+\pi^-)$ versus $m(\pi^-p)$ or $m(\pi^+p)$ reveal negligible $\Delta^0(1236)$ and $\Delta^{++}(1236)$ signals representing about 2% and less than 0.5% of the events, respectively.

C. Effective neutron-target polarization

The effective neutron-target polarization is obtained from the deuteron polarization by taking into account (1)

the Fermi motion of neutrons and the D -state component of the deuteron wave function, and (2) the probability that the event belongs to unpolarized background.

(1) For quasifree target neutrons each element of the Fermi momentum phase space corresponds to a monokinetic polarized "beam" of momentum \mathbf{p}_F and proper polarization $\mathbf{P}_n(\mathbf{p}_F)$. In our analysis we worked with neutron polarization averaged over Fermi momentum. This average $\langle \mathbf{P}_n \rangle$ depends on the details of the deuteron wave function. If the deuteron were a pure S state then $\langle \mathbf{P}_n \rangle = \mathbf{P}_d$. For a pure D -state system $\langle \mathbf{P}_n \rangle = -\frac{1}{2} \mathbf{P}_d$. We used the Reid potential¹⁶ assuming a total $D/(S+D)$ ratio of 6.44%. We have calculated $\langle \mathbf{P}_n \rangle$ for $0 \leq |\mathbf{p}_F| \leq 0.250$ GeV/c (see below), and averaged over all directions of \mathbf{p}_F . This calculation yields¹⁷ $\langle P_n \rangle = 0.963 P_d$.

In the neutron rest frame of the event α the average neutron polarization $\langle P_n \rangle$ makes a small angle $\delta(\alpha)$ with the plane perpendicular to the beam direction. The transverse polarization is thus reduced by a factor $\cos\delta(\alpha)$. The longitudinal polarization $P_L = \langle P_n \rangle \sin\delta(\alpha)$ was found to be too small to be useful for determination of longitudinal spin density matrix elements. We calculated the angles $\delta(\alpha)$ in the nonrelativistic approximation and neglected the Wigner rotation between laboratory and target rest frames.

(2) Unpolarized neutrons in the carbon and oxygen nuclei of the target material have larger average Fermi momentum than polarized neutrons in deuterons. The two distributions were measured by reconstructing events from special runs with liquid-deuterium and carbon targets. This showed that a cut at $p_F \leq 0.250$ GeV/c rejected more than one half of the background events with only a small loss in deuteron events. For the selected event α the probability $f(p_F(\alpha))$ to belong to the background was calculated from the analytical expressions fitted to the distributions for D_2 and C , respectively.

For the effective magnitude of the transverse target po-

larization for the event α we have then used

$$P_T^{\text{eff}}(\alpha) = [1 - f(p_F(\alpha))] \cos \delta(\alpha) \times 0.963 \times P_d. \quad (3.1)$$

The probability $f(p_F)$ is given by

$$f(p_F) = \frac{r D_c(p_F)}{D_d(p_F) + r D_c(p_F)}. \quad (3.2)$$

The normalized Fermi-momentum distribution $D_d(p_F)$ for deuteron is given by the Hulthen wave function

$$D_d(p_F) = \frac{4}{\pi} \alpha^2 \beta^2 (\alpha^2 + \beta^2)^3 \frac{p_F^2}{(p_F^2 + \alpha^2)^2 (p_F^2 + \beta^2)^2}, \quad (3.3)$$

where $\alpha = 0.045$ GeV/c, $\beta = 0.270$ GeV/c (Ref. 17), and $\int_0^\infty D(p_F) dp_F = 1$. We used the same form for the distribution $D_c(p_F)$ for the unpolarized neutrons in carbon and oxygen. The fitted values of the parameters in this case are $\alpha = 0.14$ GeV/c and $\beta = 0.50$ GeV/c. The factor r is

$$r = (SN_c) / N_d, \quad (3.4)$$

where N_c and N_d are the numbers of unpolarized and polarized neutrons in the target, respectively. The value of the shadow effect factor S was measured in our experiment to be $S = 0.497$. A small correction was applied to Eq. (3.2) for $p_F \leq 0.080$ GeV/c to take into account the experimental resolution of $\Delta p_F = 0.030$ GeV/c in the Fermi momentum reconstruction.

D. Acceptance of the apparatus

The acceptance in four-momentum transfer squared t covered the region $-t = 0.1 - 1.5$ (GeV/c)² at both energies. The lower limit corresponds to the minimum energy required for the proton to be detected and measured. The upper limit results from the aperture of the forward spectrometer. The acceptance was approximately the same at both energies since the longitudinal position of the spectrometer elements was scaled proportionally to the beam momentum. The cross section and acceptance yielded sufficient numbers of events for a polarization analysis in the region $-t = 0.1 - 1.0$ (GeV/c)² with the best statistics at $-t = 0.2 - 0.4$ (GeV/c)² [Fig. 4(a)]. The acceptance in the dipion invariant mass m [Fig. 4(b)] ranged from threshold to $m = 1.5$ GeV with sufficient statistics up to 1.04 GeV. The angles ψ between the transverse target polarization and the normal to the reaction plane were limited by the pole pieces of the target magnet. The recoil arms detected only events with $\psi \simeq (0 \pm 30^\circ)$ and $\psi \simeq (\pi \pm 30^\circ)$ giving optimal sensitivity for the parameters proportional to $P_T \cos \psi$ [Eq. (2.3)] and only limited sensitivity for the terms proportional to $P_T \sin \psi$. Most important for the experiment was the acceptance as a function of the dipion decay angles (θ, ϕ). The distortion of the distribution in (θ, ϕ) by the geometry of the apparatus had to be carefully studied and introduced into the analysis. In fact, only the nonuniformity of the acceptance in (θ, ϕ, ψ) has to be taken into account for the determination of normalized spin-density-matrix elements in small regions (t, m). Variation of acceptance as a function of t and m is relevant only for calculation of unnormalized spin-density-matrix elements in different (t, m) bins.

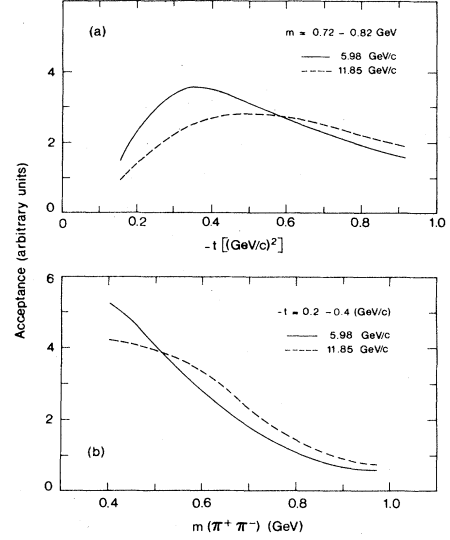


FIG. 4. The t dependence and the mass dependence of geometrical acceptance integrated over the true angular distribution in θ , ϕ , and ψ at 5.98 and 11.85 GeV/c.

For each (t, m) bin used in the analysis a high-statistics sample of Monte Carlo events was generated uniformly in (t, m, θ, ϕ, ψ) with distributions following closely those of the real events for the incident particle momentum and direction, the vertex position in the target, the target Fermi momentum, the energy loss, and the multiple scattering of the produced particles. The produced pions were allowed to decay and the decay muon was tracked through the apparatus. The Monte Carlo events were then reconstructed and fitted like the real events, and the acceptance coefficients (4.2) were calculated for each term of the expression (2.3).

The estimate of the acceptance corrected cross sections is shown in Fig. 5. The relative normalization of different (t, m) bins was determined only approximately since it does not enter our analysis in terms of normalized observables in each bin. However, the skewing of the ρ mass

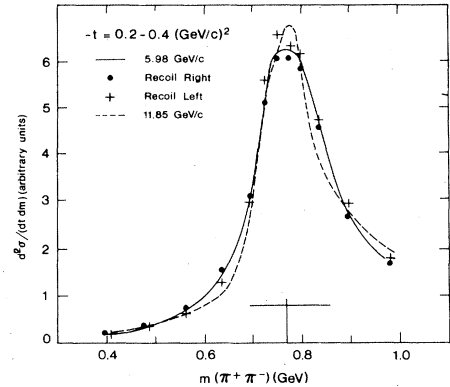


FIG. 5. Approximate results for the mass dependence of the unpolarized cross section $d^2\sigma/(dt dm)$ at 5.98 and 11.85 GeV/c. Events detected in different parts of the apparatus yield consistent results [see Sec. IV B (1)].

peak and the difference in shape at 5.98 and 11.85 GeV/ c , respectively, are real effects and are discussed in Sec. V D.

IV. DATA ANALYSIS

The aim of the experiment is to determine the average values of normalized spin-density-matrix elements in small regions of four-momentum transfer squared $-t$ and dipion invariant mass m . All events within a sufficiently small (t, m) bin are assumed to be produced with the same angular distribution $W(\theta, \phi, \psi)$ (2.3).

Since the target-polarization-independent parameters are obtained with small statistical errors their dependence on t and m can be studied in narrow bins whereas the determination of matrix elements of type ρ^y or ρ^x requires larger bins with at least $\simeq 1000$ events. Convolution of cross section and acceptance gives the highest statistics for $-t=0.2-0.4$ (GeV/ c)² and, as function of mass, in the ρ^0 peak. This led us to analyze the same events in different sets of (t, m) bins: (1) The t dependence in the ρ^0 mass range $m=0.720-0.820$ GeV, (2) the m dependence for $-t=0.2-0.4$ (GeV/ c)², and (3) the m and t dependence in the full accessible kinematic range. In the following we discuss the details of the maximum-likelihood fit used to determine the spin-density-matrix elements and the consistency tests in our analysis.

A. The maximum-likelihood function

The maximum-likelihood function $L'(a)$ for determining the parameters a_2, \dots, a_{15} in the expression (2.5) from events α' obeying the *produced* angular distribution, i.e., undistorted by acceptance or pion decay, is given by

$$L'(a) = \prod_{\alpha'} \left[1 + \sum_{i=2}^{15} a_i c_i(\alpha') Y_i(\theta_{\alpha'}, \phi_{\alpha'}) \right] \quad (4.1)$$

with

$$c_i(\alpha') = \begin{cases} 1 & \text{for } i=2, \dots, 6 \\ P_T^{\text{eff}}(\cos\psi)_{\alpha'} & \text{for } i=7, \dots, 12 \\ P_T^{\text{eff}}(\sin\psi)_{\alpha'} & \text{for } i=13, 14, 15. \end{cases}$$

Various methods to take into account the acceptance of the apparatus are discussed in the literature.^{18,19} In our data analysis we proceed as follows. From the Monte Carlo events we calculate for each parameter a_i , $i=2, 3, \dots, 15$ an acceptance coefficient ϵ_i

$$\epsilon_i = \frac{\sum_{\beta} c_i(\beta) Y_i(\theta_{\beta}, \phi_{\beta})}{\sum_{\beta} c_1(\beta) Y_1(\theta_{\beta}, \phi_{\beta})}, \quad (4.2)$$

where \sum_{β} is the sum over all “observed” Monte Carlo events β in the particular (t, m) bin and where the coefficients c_i are defined in (4.1). The denominator in (4.2) is simply the ratio between the numbers of “observed” and generated Monte Carlo events. To obtain the measured parameters from the *accepted* real events α we introduce the acceptance coefficients ϵ_i into the maximum-likelihood function in a way which restores the independence of the normalization of $W(\theta, \phi, \psi)$ on the parameters.¹⁸

$$L(a) = \prod_{\alpha} \frac{1 + \sum_{i=2}^{15} a_i c_i(\alpha) Y_i(\theta_{\alpha}, \phi_{\alpha})}{1 + \sum_{i=2}^{15} a_i c_i(\alpha) \epsilon_i} \equiv \prod_{\alpha} R_{\alpha}. \quad (4.3)$$

This method is appropriate to our analysis which assumes that only a limited number of terms is present in the distribution function.

The runs with opposite signs of target polarization are normalized with respect to each other by coefficients e^+ and e^- . The different methods used to determine e^+ and e^- have been described elsewhere.¹ These coefficients, of the order of (1.00 ± 0.01) , are introduced in the likelihood function as weights

$$L(a) = \prod_{\alpha} (R_{\alpha})^{e_{\alpha}}, \quad (4.4)$$

where $e_{\alpha} = e^+$ or $e_{\alpha} = e^-$, depending on the sign of the target polarization for event α .

The experiment also yields directly the “left-right asymmetry” for production on polarized neutrons, i.e., the relative change of cross section to one side when reversing the sign of target polarization. This method is insensitive to differences in left and right acceptances. This asymmetry is given by

$$A = \frac{n^+ - n^-}{(n^+ - n_f) P_t^+ + (n^- - n_f) P_t^-}, \quad (4.5)$$

where n^+ and n^- are the normalized numbers of events for positive (P_t^+) and negative (P_t^-) target polarizations and where n_f is the normalized number of events from unpolarized neutrons determined by runs with carbon target. The parameter a_7 in Eq. (3.5) is equal to the asymmetry A . In our analysis we therefore introduce the measured value $(A \pm \Delta A)$ as a constraint on a_7 :

$$L(a) = \exp \left[-\frac{(a_7 - A)^2}{(\Delta A)^2} \right] \prod_{\alpha} (R_{\alpha})^{e_{\alpha}}. \quad (4.6)$$

The consistency between the unconstrained results for a_7 and the direct measurement of A has been verified in bins of high statistics. A similar relation exists between a_{15} and the “up-down asymmetry” but was not used.

The expression (4.6) for the maximum-likelihood function was used to determine the parameters from the observed events in each (t, m) bin. The CERN optimization program FUMILI was run at the Saclay CDC 7600. The CERN program MINUIT yields essentially the same results.

The optimization of the likelihood function $L(a)$ should in principle take into account the constraints on the spin-density-matrix elements imposed by positivity conditions, Schwartz inequalities, and nonlinear inequalities of La France–Winternitz type.²⁰ The hypothesis of S and P -wave dominance introduces additional constraints. Imposing constraints during the optimization involves methods of nonlinear programming.²¹ The presented results were obtained by standard unconstrained optimization. Constraints based on the S - and P -wave dominance were tested and found to be satisfied within the quoted errors in most (t, m) bins.

B. The consistency tests

Our analysis was subjected to the following consistency tests.

(1) Consistency of results when analyzing separately events with recoil to the left and to the right. The two samples involve to a large extent different detectors. The test therefore checks the effects of local inefficiencies or errors. Also, any error in relative normalization of runs with positive and negative target polarization would appear with opposite sign in the results thus leading to an inconsistency. Furthermore, discrimination against background from events with undetected additional pions is different for the two samples.

(2) Consistency of the results for the target-polarization-independent parameters obtained either with deuterated propanediol polarized target or with carbon target. This test confirms validity of the assumption that the interactions take place on quasifree neutrons. The test also checks the relative normalization of runs with positive and negative target polarization.

(3) Independence of results for $\rho_{ss}^y + \rho_{00}^y + 2\rho_{11}^y$ and for ρ_{1s}^x on the choice of the dipion s - or t -channel helicity frames. Strong variations of matrix elements or acceptance within a given (t, m) bin could lead to different results. We observe only negligible differences in these s - and t -channel invariants.

(4) The method used to calculate the acceptance coefficients was checked for the target polarization independent parameters a_2, \dots, a_6 by calculating their values using as input the Monte Carlo events accepted by our model for the apparatus and retained after standard reconstruction and fitting procedure. The results are consistent with zero for all five parameters, in accordance with the originally isotropic distribution in (θ, ϕ) . Additional check of our acceptance calculation is the good agreement between our results for the target-polarization-independent parameters at 5.98 GeV/c and those of Wicklund *et al.*⁵ at 6 GeV/c using the Argonne effective-mass spectrometer with different geometrical acceptance.

All of these tests were carried out using the S - and P -wave approximation for $W(\theta, \phi, \psi)$. Two more consistency checks were performed allowing for additional terms.

(5) Six terms proportional to imaginary parts of $\rho_{1s}, \rho_{1-1}, \rho_{10}$ and $\rho_{1s}^y, \rho_{1-1}^y, \rho_{10}^y$ were added. The nonzero values of the order of a few percent for some of these parameters are to be considered as due to small systematic errors in apparatus or analysis rather than as evidence for parity violation. The first 14 parameters remain however practically unchanged with respect to the results of the standard S - and P -wave analysis.

(6) Six terms of higher order in θ , proportional to linear combinations of interference terms between dominating P -wave amplitudes and D -wave amplitudes with dimeson helicities 0 or 1 are added in the expansion of $W(\theta, \phi, \psi)$. These terms are

$$\begin{aligned} &\langle \text{Re}Y_0^3 \rangle, \langle \text{Re}Y_1^3 \rangle, \langle \text{Re}Y_2^3 \rangle, \\ &\langle P_T \cos\psi \text{Re}Y_0^3 \rangle, \langle P_T \cos\psi \text{Re}Y_1^3 \rangle, \\ &\langle P_T \cos\psi \text{Re}Y_2^3 \rangle. \end{aligned}$$

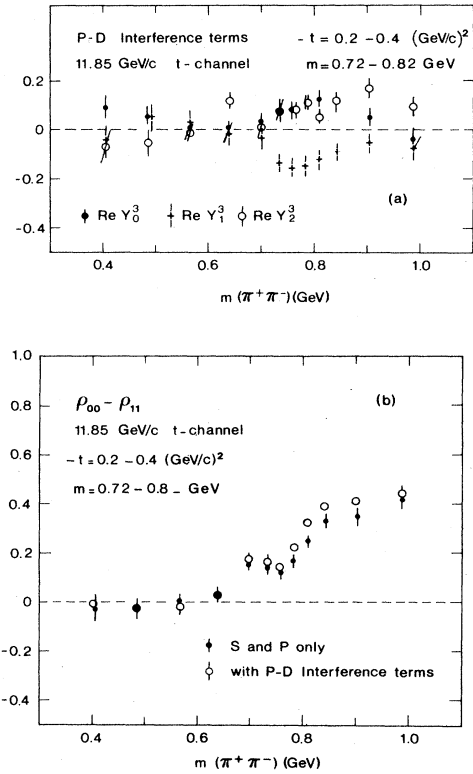


FIG. 6. Search for D waves: (a) P - and D -wave interference terms in the t channel at 11.85 GeV/c; (b) Sensitivity of $(\rho_{00} - \rho_{11})$ to the presence of P - D interference terms.

Significant nonzero values for these terms were found only at 11.85 GeV/c and for $m \geq 0.7$ GeV and are shown in Fig. 6(a) (see also Tables 4 and 20 of Ref. 14). The corresponding change in the value of the S - and P -wave parameters is negligibly small (within statistical errors) except for $\rho_{00} - \rho_{11}$ at 11.85 GeV/c and $m \geq 0.7$ GeV [Fig. 6(b)]. We conclude that, with this exception, the S - and P -wave approximation introduces systematic errors which are smaller than the quoted statistical errors.

V. EXPERIMENTAL RESULTS AND DISCUSSION

A. Spin-density-matrix elements

Average values of the 14 observed spin-density-matrix (SDM) elements were measured in small bins of (t, m) , in both t -channel and s -channel dipion helicity frames. All results are given in Ref. 14.

In Fig. 7 we show the t -dependence of the t -channel SDM elements at the ρ^0 mass for the incident momentum 5.98 GeV/c. Results at 11.85 GeV/c have similar t dependence but a comparison with those at 5.98 GeV/c shows evidence for energy dependence of some of the parameters. This is also evident when we compare in Fig. 7 our data at 5.98 GeV/c with those for $\pi^-p \rightarrow \pi^+\pi^-n$ at 17.2 GeV/c (Ref. 6). The mass dependence of the SDM elements is shown in Fig. 8 for $-t = 0.20 - 0.40$ (GeV/c)².

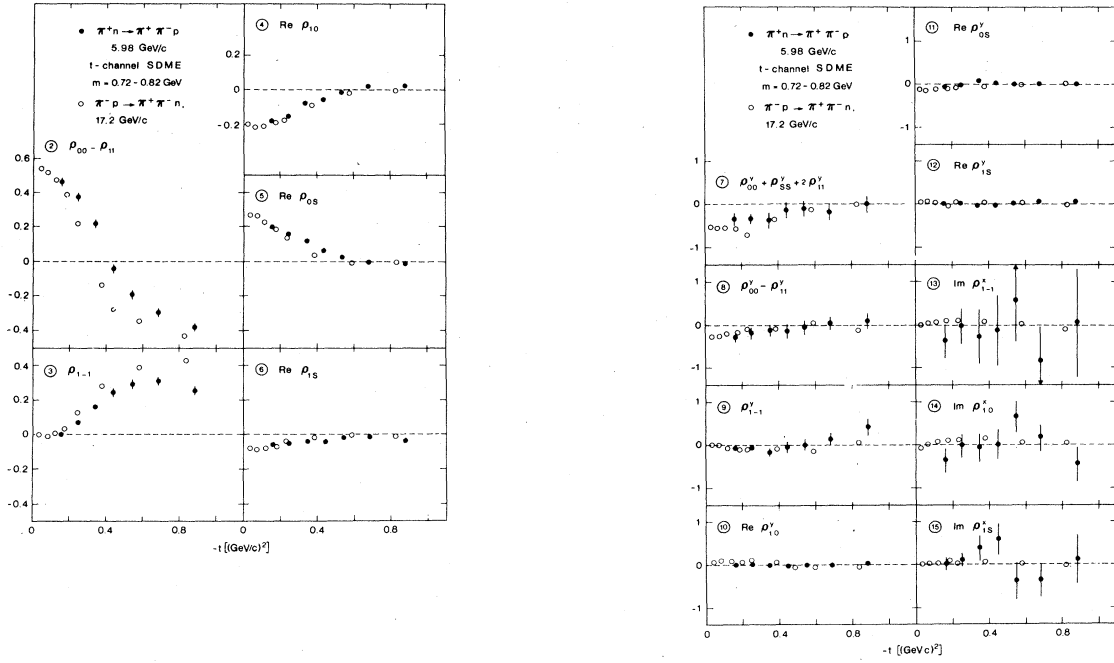


FIG. 7. Normalized spin-density-matrix elements at 5.98 GeV/c as a function of $-t$ in the ρ^0 mass region. The CERN results for $\pi^- p_1 \rightarrow \pi^- \pi^+ \pi^- n$ at 17.2 GeV/c and at $m(\pi^+ \pi^-) = 0.71-0.83$ GeV are shown for comparison.

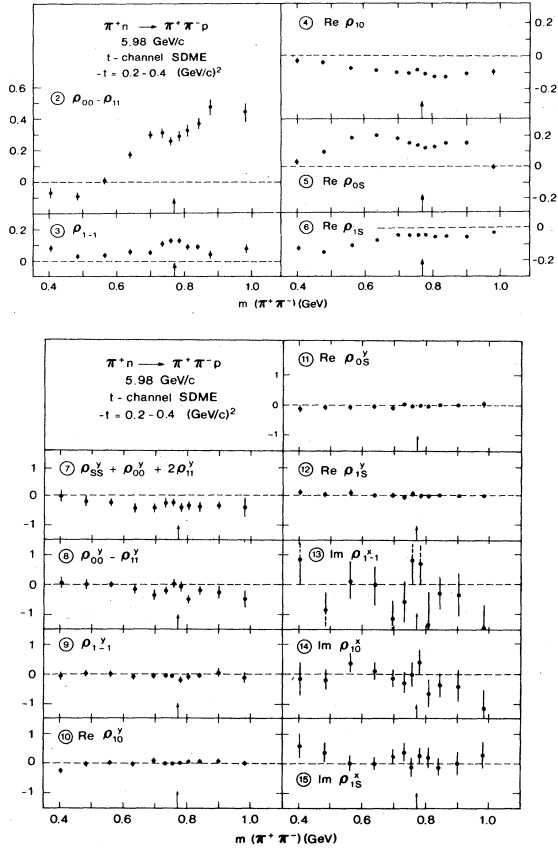


FIG. 8. Normalized spin-density-matrix elements at 5.98 GeV/c as a function of the $(\pi^+ \pi^-)$ invariant mass m for $-t = 0.2-0.4$ (GeV/c) 2 . The arrows indicate the ρ^0 mass.

All measured polarization-dependent SDM elements are nucleon-helicity-flip-nonflip interference terms. It is instructive to show their explicit form in terms of amplitudes with definite naturality (2.7). With $\Sigma = d^2 \sigma / (dt dm)$ these relations read^{10,11,13}

$$\begin{aligned} (\rho_{ss}^y + \rho_{00}^y + 2\rho_{11}^y) \Sigma &= 2\text{Im}(S_0 S_1^* + L_0 L_1^* + U_0 U_1^* + N_0 N_1^*), \\ (\rho_{00}^y - \rho_{11}^y) \Sigma &= \text{Im}(2L_0 L_1^* - U_0 U_1^* - N_0 N_1^*), \end{aligned} \quad (5.1a)$$

$$\rho_{1-1}^y \Sigma = \text{Im}(N_0 N_1^* - U_0 U_1^*),$$

$$\sqrt{2} \text{Re} \rho_{10}^y \Sigma = \text{Im}(U_0 L_1^* - U_1 L_0^*),$$

$$\sqrt{2} \text{Re} \rho_{15}^y \Sigma = \text{Im}(U_0 S_1^* - U_1 S_0^*), \quad (5.1b)$$

$$\text{Re} \rho_{05}^y \Sigma = \text{Im}(L_0 S_1^* - L_1 S_0^*),$$

$$-\text{Im} \rho_{1-1}^x \Sigma = \text{Im}(N_0 U_1^* + N_1 U_0^*),$$

$$\sqrt{2} \text{Im} \rho_{10}^x \Sigma = \text{Im}(N_0 L_1^* + N_1 L_0^*), \quad (5.1c)$$

$$\sqrt{2} \text{Im} \rho_{15}^x \Sigma = \text{Im}(N_0 S_1^* + N_1 S_0^*).$$

The parameters (5.1a) all have different nonzero values. This means that at least two of the three nonflip amplitudes S_0, L_0, U_0 (“ A_1 ” exchange) are nonzero and have phases different from the corresponding flip amplitudes S_1, L_1, U_1 (“ π ” exchange). The small but nonzero values of parameters (5.1b) confirm this conclusion. These results invalidate the assumption of the complete absence of A_1 exchange which was frequently made in the analyses of $\pi\pi$ production and $\pi\pi$ scattering from unpolarized data.⁷ Finally, the nonzero values of (5.1c) confirm the

expectation that natural and unnatural exchange amplitudes have different phases.

B. Normalized partial-wave cross sections and recoil polarizations

While a complete separation of S - and P -wave contributions require a full amplitude analysis¹³ we will make use in the following of the fact that six of the measured SDM elements are simple linear combinations of the moduli squared of the eight recoil transversity amplitudes (RTA) defined in (2.8). We will work with normalized RTA corresponding to $\Sigma \equiv d^2\sigma/(dt dm)=1$ and define normalized partial-wave cross sections and recoil polarizations for amplitudes $A=S,L,U,N$ as

$$\sigma(A) = |A|^2 + |\bar{A}|^2, \quad \tau(A) = |A|^2 - |\bar{A}|^2. \quad (5.2)$$

Then we get

$$\rho_{ss} + \rho_{00} + 2\rho_{11} = \sigma(S) + \sigma(L) + \sigma(U) + \sigma(N),$$

$$\rho_{00} - \rho_{11} = \sigma(L) - \frac{1}{2}[\sigma(U) + \sigma(N)], \quad (5.3)$$

$$\rho_{1-1} = -\frac{1}{2}[\sigma(U) - \sigma(N)],$$

$$\rho_{ss}^y + \rho_{00}^y + 2\rho_{11}^y = \tau(S) + \tau(L) + \tau(U) - \tau(N),$$

$$\rho_{00}^y - \rho_{11}^y = \tau(L) - \frac{1}{2}[\tau(U) - \tau(N)], \quad (5.4)$$

$$\rho_{1-1}^y = -\frac{1}{2}[\tau(U) + \tau(N)].$$

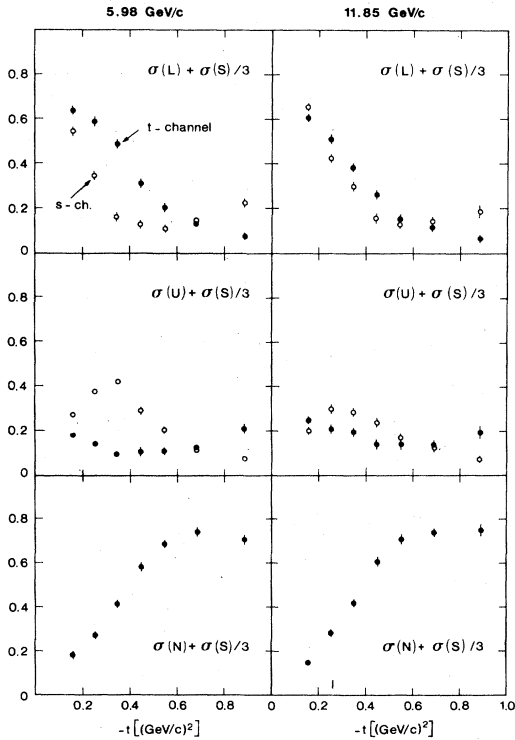


FIG. 9. Three linear combinations of the normalized partial-wave cross sections as a function of $-t$ in the ρ^0 mass region $m=0.720-0.820$ GeV. Note that $\sigma(S)$ and $\sigma(N)$ are invariant under transformation from the t -channel to the s -channel dipion helicity frame of reference.

From the six equations (5.3) and (5.4) we calculate¹⁴ six mixed normalized partial cross sections and recoil polarizations:

$$\sigma(L) + \frac{1}{3}\sigma(S), \quad \sigma(U) + \frac{1}{3}\sigma(S), \quad \sigma(N) + \frac{1}{3}\sigma(S), \quad (5.5)$$

$$\tau(L) + \frac{1}{3}\tau(S), \quad \tau(U) + \frac{1}{3}\tau(S), \quad -\tau(N) + \frac{1}{3}\tau(S).$$

The results are shown in Figs. 9 and 10 as a function of $-t$ in the ρ^0 mass region. We observe the expected dominance of $[\sigma(L) + \frac{1}{3}\sigma(S)]$ at small t and its rapid decrease with t . For $|t| \geq 0.5$ the natural exchange contribution dominates. We note a change of sign of $[-\tau(N) + (1/3)\tau(S)]$ near $-t \simeq 0.5$. We discuss this point in Sec. V C.

To study in more detail the relative contribution of the natural exchange amplitudes we examine the ratio

$$R = \frac{\sigma(N) + \frac{1}{3}\sigma(S)}{\sigma(U) + \sigma(L) + \frac{2}{3}\sigma(S)}. \quad (5.6)$$

This ratio does not depend on the choice of the s - or t -channel helicity frame of reference. Close to the dipion threshold $m=0.28$ GeV this ratio must approach $R = \frac{1}{2}$. Our results are shown in Fig. 11. Note that $R > \frac{1}{2}$ implies $\sigma(N) > \frac{1}{2}[\sigma(L) + \sigma(U)]$. For small t the ratio decreases with m . This is consistent with theoretical expectations based on off-shell finite-energy sum rules defined for amplitudes describing scattering of Reggeon + particle \rightarrow particle + particle.^{8,9} However at large t we observe a peak in $R(m)$ at the ρ^0 mass which has not been theoretically expected.

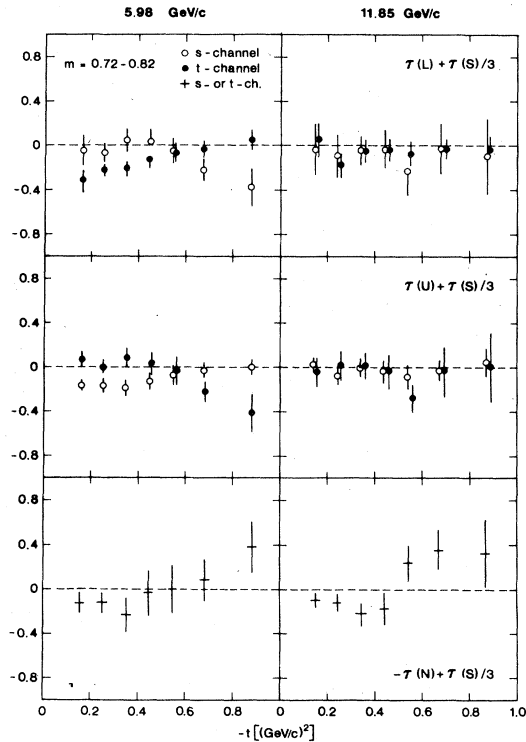


FIG. 10. Three linear combinations of the normalized partial-wave recoil polarizations as a function of $-t$ in the ρ^0 mass region $m=0.720-0.820$ GeV.

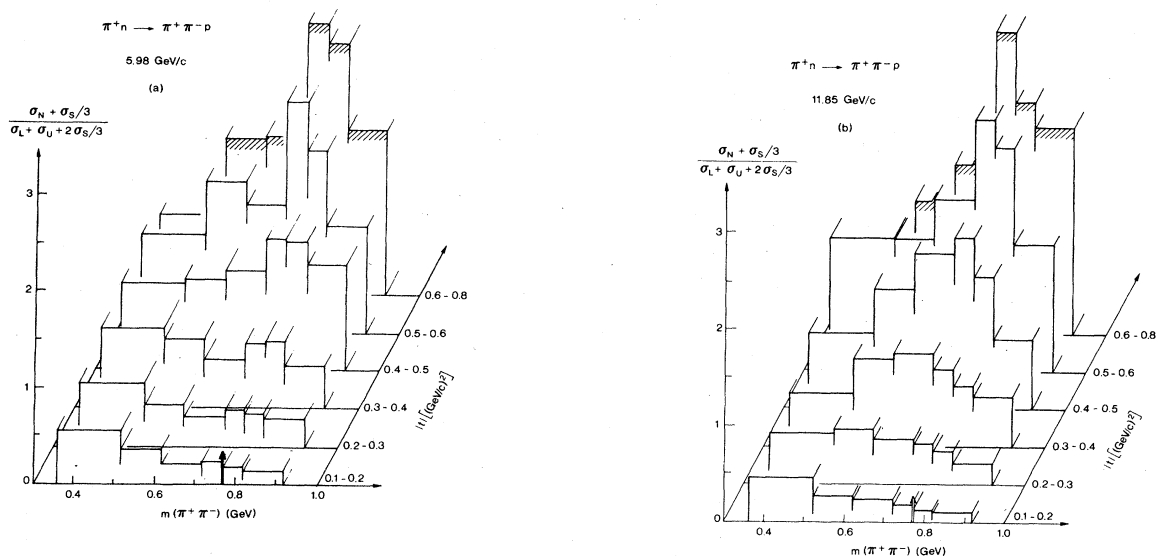


FIG. 11. The ratio of frame invariant components A and B of the cross section $d^2\sigma/(dt dm)$ [Eq. (5.10)] as a function of both $-t$ and the dipion invariant mass m at (a) 5.98 GeV/c and (b) 11.85 GeV/c.

C. Bounds on moduli of recoil transversity amplitudes

Equations (5.3) and (5.4) can also be solved in terms of the following combinations of moduli squared of RTA:

$$\begin{aligned} |L|^2 + \frac{1}{3}|S|^2, \quad |U|^2 + \frac{1}{3}|S|^2, \quad |N|^2 + \frac{1}{3}|\bar{S}|^2, \\ |\bar{L}|^2 + \frac{1}{3}|\bar{S}|^2, \quad |\bar{U}|^2 + \frac{1}{3}|\bar{S}|^2, \quad |\bar{N}|^2 + \frac{1}{3}|S|^2. \end{aligned} \quad (5.7)$$

$$\left(\frac{1}{3}|S|^2\right)_{\text{upper}} = \text{Min}_{s \text{ and } t} \left\{ |L|^2 + \frac{1}{3}|S|^2, |U|^2 + \frac{1}{3}|S|^2, |\bar{N}|^2 + \frac{1}{3}|S|^2 \right\},$$

$$\left(\frac{1}{3}|\bar{S}|^2\right)_{\text{upper}} = \text{Min}_{s \text{ and } t} \left\{ |\bar{L}|^2 + \frac{1}{3}|\bar{S}|^2, |\bar{U}|^2 + \frac{1}{3}|\bar{S}|^2, |\bar{N}|^2 + \frac{1}{3}|S|^2 \right\}. \quad (5.8)$$

These bounds allow an immediate discussion of the structure of amplitudes in advance of detailed amplitude analysis. The bounds at 5.98 GeV/c are presented in Fig. 12 and Fig. 13 showing their t dependence and m dependence, respectively. The results at 11.85 GeV/c are similar. Only the mean values of the bounds are shown for clarity. The essential features of the amplitudes discussed below are valid within the statistical errors on the bounds and are all confirmed by the exact amplitude analysis.¹³

Before we discuss our results for these bounds we note that when $|A| \neq |\bar{A}|$ then both amplitudes A_0 and A_1 are nonzero and must have different phases. If $|A| \simeq |\bar{A}|$ then one of the amplitudes A_0 and A_1 is small or vanishing, or both amplitudes have the same phase.

We first comment on the t dependence of the amplitudes in the ρ^0 resonance mass region (Fig. 12). The large differences between $|L|^2$ and $|\bar{L}|^2$ for $-t \geq 0.6$ (GeV/c)² and between $|U|^2$ and $|\bar{U}|^2$ for $-t \leq 0.6$ (GeV/c)² indicate substantial contribution from the

Our results for (5.7) in both s - and t -channel dimeson helicity frames are given in Ref. 14. Note that the amplitudes S, \bar{S}, N, \bar{N} are invariant under s -to- t -channel crossing transformations.

The results obtained for (5.7) can be taken as upper bounds on moduli squared of P -wave RTA. The lower bounds are obtained by subtracting from the terms in (5.7) an upper bound on $\frac{1}{3}|S|^2$ or $\frac{1}{3}|\bar{S}|^2$. In each (t, m) bin we calculate

“ A_1 ”-exchange amplitudes L_0 and U_0 with phases different from the “ π ”-exchange amplitudes L_1 and U_1 . However, for $-t \leq 0.6$ (GeV/c)² the amplitude L_0 is either small or it is in phase with the amplitude L_1 . The same conclusion holds true for the amplitude U_0 for $-t \geq 0.6$ (GeV/c)². The large differences between $|N|^2$ and $|\bar{N}|^2$ indicate that the “ A_2 ”-exchange amplitudes N_0 and N_1 must have different structures.

The crossing of $|N|^2$ and $|\bar{N}|^2$ near $-t \simeq 0.45$ (GeV/c)² [see Fig. 12(c)] is due to the change of sign of $\text{Im}(N_0 N_1^*)$. We note that the data on polarization in $\pi^- p \rightarrow \eta n$ at 7.85 GeV/c, a reaction which proceeds by pure A_2 exchange, also show such a change of sign.²² The construction of A_2 exchange amplitudes from $\bar{K}N$ and $\bar{K}N$ charge-exchange polarization data²³ at 6 GeV/c produces a nonflip amplitude that vanishes near $-t \simeq 0.45$ (GeV/c)² with the $\text{Re}N_0$ changing sign and $\text{Im}N_0$ having a double zero structure. The same conclusion was reached from a simultaneous analysis²⁴ of $\pi^- p \rightarrow \pi^0 n$, $\rightarrow \eta n$, and $\rightarrow K^0 n$ reactions at 6 GeV/c. We

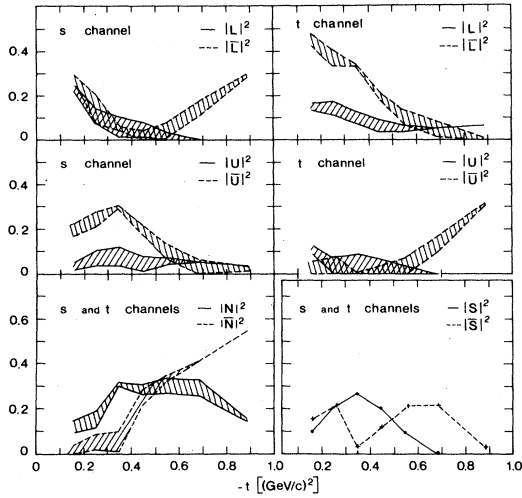


FIG. 12. The t dependence of the lower and upper bounds on the moduli squared of the normalized P -wave recoil transversity amplitudes for $m=0.720\text{--}0.820$ GeV at 5.98 GeV/c. Also shown are the upper bounds for the normalized S -wave amplitudes.

suggest that N_0 in $\pi^+n \rightarrow \rho^0 p$ has the same structure. We find a similar crossover¹⁴ of $|N|^2$ and $|\bar{N}|^2$ at 11.85 GeV/c. However, the CERN-Munich-Cracow amplitudes at 17.2 GeV/c do not show this behavior in Ref. 6.

The mass dependence of the bounds in the region $-t=0.2\text{--}0.4$ (GeV/c)² shows interesting structures (Fig. 13). In general, the unnatural exchange amplitudes with the transversity down are larger than those with the transversity up in both channels. The opposite is true for the natural exchange amplitudes: the transversity “up” is the larger amplitude. In the narrow vicinity of the ρ^0 mass all P -wave transversity-up amplitudes have a peak while the transversity-down amplitudes show a dip. In the s channel, this structure is less pronounced in the dipion helicity $m=0$ amplitudes $|L|^2$ and $|\bar{L}|^2$ but it is

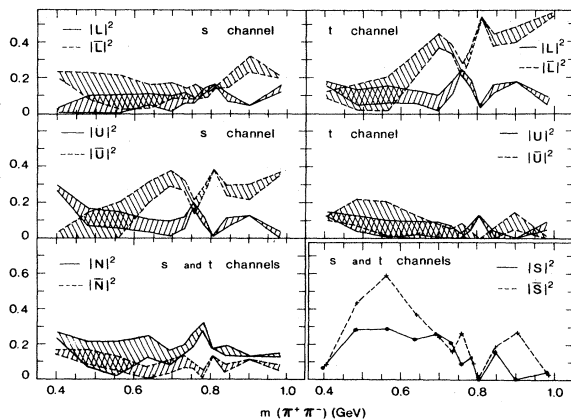


FIG. 13. The m dependence of the lower and upper bounds on the moduli squared of the normalized P -wave recoil transversity amplitudes for $-t=0.20\text{--}0.40$ (GeV/c)² at 5.98 GeV/c, and the upper bounds for the normalized S -wave moduli squared.

evident in the amplitudes with dipion helicity $m=\pm 1$. The dip in $|\bar{U}|^2$ and $|\bar{N}|^2$ also shows up clearly when the bounds are multiplied by the cross section $d^2\sigma/(dt dm)$.

We conclude that the production of $J=1$ $\pi^+\pi^-$ state at the ρ^0 mass proceeds via unnatural exchange with about equal contributions from the amplitudes with transversities “up” and “down” ($|L|^2 \simeq |\bar{L}|^2$ and $|U|^2 \simeq |\bar{U}|^2$). This contrasts with the production via the natural exchange which is dominated by the transversity-“up” amplitude N while the transversity-“down” amplitude \bar{N} is small or zero.

The structures observed in the mass region 0.700–0.840 GeV show that the shape of the ρ^0 peak in the spin-averaged cross section $d^2\sigma/(dt dm)$ is not reproduced in the moduli squared of individual amplitudes. These structures are not due to ρ - ω interference which concerns a narrow mass interval of 0.770–0.800 GeV and leads to effects of the order of the quoted errors. The structures are statistically significant. Our statistics are large in this kinematic region and the statistical errors are small. The large dip in the s channel $|\bar{U}|^2$ and the t channel $|\bar{L}|^2$ are well established within two standard deviations (2σ). The peaks in the s -channel $|U|^2$, $|N|^2$ and the t -channel $|\bar{L}|^2$ are established within $1.5\sigma\text{--}2\sigma$. The dip in $|\bar{N}|^2$ at $\simeq 0.780$ GeV is certain only within 1σ because of the overall small magnitude of this amplitude. Our study¹⁴ of the mass dependence in smaller bins of t has shown that the conclusions presented here for $-t=0.2\text{--}0.4$ (GeV/c)² are most appropriate for the interval $-t=0.2\text{--}0.3$ (GeV/c)².

In the following we restrict our discussion to the s channel and examine the results in Fig. 13 in terms of nucleon helicity nonflip and flip amplitudes (2.7)

$$2|A|^2 = |A_0|^2 + |A_1|^2 + 2\epsilon \text{Im}(A_0 A_1^*), \quad (5.9)$$

$$2|\bar{A}|^2 = |A_0|^2 + |A_1|^2 - 2\epsilon \text{Im}(A_0 A_1^*),$$

where $\epsilon = +1$ for $A=S, L, U$ and $\epsilon = -1$ for $A=N$.

The relative magnitudes of $|A|^2$ and $|\bar{A}|^2$ imply that the relative phase $\Phi_A = \Phi_{A_0} - \Phi_{A_1}$ between all amplitudes A_0 and A_1 is negative ($\sin\Phi_A \leq 0$) except for Φ_U at $m \leq 0.6$ GeV. The bounds show that the amplitudes L_0 and L_1 are nearly in phase and at the ρ^0 mass their phases are equal. For the amplitudes U_0 and U_1 the magnitude of $\sin\Phi_U$ is large and the amplitudes are near 90° out of phase. However their relative phase changes rapidly near the ρ^0 mass and at the ρ^0 mass the amplitudes U_0 and U_1 have the same phase. For the amplitudes N_0 and N_1 the magnitude of $\sin\Phi_N$ is small outside the ρ^0 range. However, their relative phase also changes rapidly near the ρ^0 mass and at the ρ^0 mass the amplitudes N_0 and N_1 are about 90° out of phase.

An alternative interpretation can be given in terms of magnitudes of the amplitudes A_n , $n=0,1$. The behavior of $|L|^2$ and $|\bar{L}|^2$ is consistent with an amplitude L_0 which is small for $m \leq 0.7$, vanishes at the ρ^0 mass and becomes large for $m \geq 0.85$. The behavior of $|U|^2$ and $|\bar{U}|^2$ suggests that the amplitude U_0 is large and out of phase with U_1 except near the ρ^0 mass where U_0 vanishes. This possibility would mean that the production of

$\pi^+\pi^-$ proceeds at the ρ^0 mass via unnatural exchange essentially with nucleon helicity flip: while the amplitudes L_1 and U_1 resonate, the amplitudes L_0 and U_0 vanish or are very small. At the same time the amplitudes N_0 and N_1 both resonate, have about equal amplitudes but are about 90° out of phase. It is also possible that the two interpretations apply differently to the dipion helicity $m=0$ amplitudes L_0 and L_1 and to the $m=\pm 1$ amplitudes U_0 and U_1 . Our experiment cannot select between these various possibilities.

The $\pi^+\pi^-$ state crossing angle χ between the s - and t -channel helicity frames in the kinematic region of Fig. 13 is such that $\sin\chi$ is near 1 but $\sin 2\chi$ is still large. The results for the bounds in the t channel then suggest that the relative phase between L and U amplitudes in the s channel is not large. This is confirmed in the detailed amplitude analysis.¹³

Finally we note that the bounds on the normalized S -wave transversity amplitudes, when multiplied by the cross section $d^2\sigma/(dt dm)$, do not exclude a possible S -wave resonance in the mass region 0.7 to 0.8 GeV.

D. Shape of the ρ^0 peak in the physical region of t

The structures in the mass dependence of the recoil transversity amplitudes manifest themselves as differences in the shape of the ρ^0 peak in the measured helicity-frame invariant components of the cross section

$$A = [\sigma(N) + \frac{1}{3}\sigma(S)]d^2\sigma/(dt dm), \quad (5.10)$$

$$B = [\sigma(L) + \sigma(U) + \frac{2}{3}\sigma(S)]d^2\sigma/(dt dm).$$

We also define

$$I(a) = \sigma(a)d^2\sigma/(dt dm), \quad a = S, L, U, N. \quad (5.11)$$

To evaluate (5.10) and (5.11) we used the approximate values of the cross section shown in Fig. 5. We find that at all values of t and at both energies, A presents a ρ^0 peak which is narrower by 10 to 20% and shifted toward lower masses by 10 to 15 MeV with respect to B (see Fig. 14). The ratio of the two components in a given bin is an exact result of our analysis whereas the relative normalization of different bins is only approximate. The effect is due to the P wave and not to the S wave. This is verified by looking at

$$B - 2A = I(L) + I(U) - 2I(N),$$

which shows the mass dependence as expected from Fig. 14.

The statistical significance of the effect is shown best by examining in the s channel the differences

$$I(N) - I(U) = 2\rho_{1-1}d^2\sigma/(dt dm), \quad (5.12)$$

$$I(U) - I(L) = \{[\sigma(U) + \frac{1}{3}\sigma(S)] - [\sigma(L) + \frac{1}{3}\sigma(S)]\} \\ \times d^2\sigma/(dt dm).$$

The mass dependence of $I(U) - I(N)$ is presented in Fig. 15(a). It confirms that the ρ^0 is wider in $I(U)$ than in $I(N)$. The mass dependence of $I(U) - I(L)$ is shown in

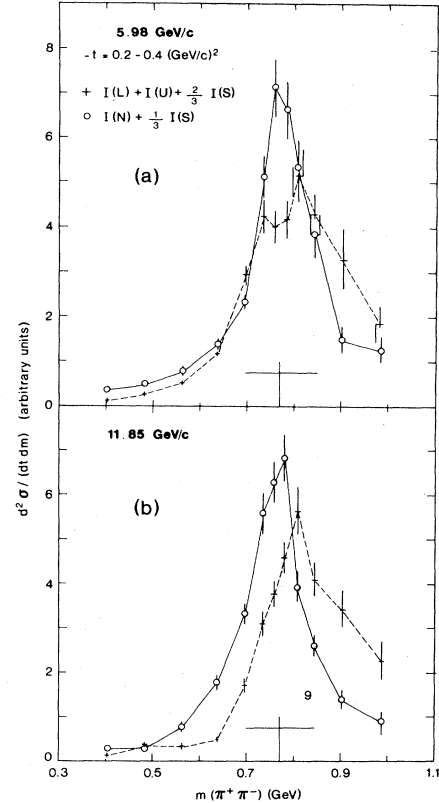


FIG. 14. The m dependence of frame-invariant components A and B of the cross section $d^2\sigma/(dt dm)$ [Eq. (5.10)] at (a) 5.98 GeV/c and (b) 11.85 GeV/c. In order to emphasize the difference in shape and position of the ρ^0 peak the histograms for the two components are normalized to the same area. The cross indicates the standard ρ^0 (Ref. 27) at the pion pole.

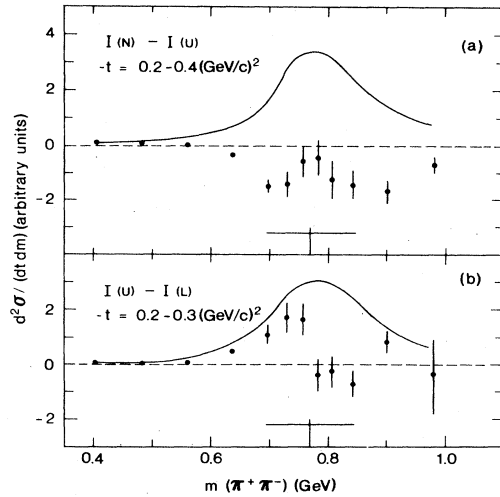


FIG. 15. The m dependence of the difference between individual P -wave cross sections given directly by the measured observables; (a) $I(N) - I(U)$ and (b) $I(U) - I(L)$. The curves show the spin-averaged cross section $d^2\sigma/(dt dm)$ in the same intervals of (a) $-t = 0.2 - 0.4$ (GeV/c)² and (b) $-t = 0.2 - 0.3$ (GeV/c)², respectively.

Fig. 15(b). At $-t=0.2-0.3$ where the contributions from the L and U amplitudes are about equal, this difference changes sign at $m=0.770$ GeV. This means that the ρ^0 peak in $I(U)$ is shifted toward lower masses compared to $I(L)$.

To understand qualitatively these differences in the position and shape of the ρ^0 peak let us consider any P -wave recoil transversity amplitude $A(s,t,m^2)$ as a function of the complex dipion mass z . In the real mass vicinity of the ρ^0 complex pole $z_\rho = m_\rho^2 - i\gamma$ we can write

$$A(s,t,m^2) = \frac{R(s,t,z_\rho)}{m^2 - z_\rho} + Q(s,t,m^2), \quad (5.13)$$

where $R(s,t,z_\rho)$ is the pole residue and $Q(s,t,m^2)$ is the background analytic near z_ρ . The pole residue can be factorized $R = F(s,t,z_\rho)f(z_\rho)$ where F and f are amplitudes for $\pi^+n \rightarrow \rho^0 p$ and $\rho^0 \rightarrow \pi^+\pi^-$, respectively. The residues R modulate the width of the resonance peak in each transversity amplitude. The interference of the pole with the background term could produce the small shifts in the apparent position of the ρ^0 peak discussed above. In contrast to the amplitudes $F(s,t,z_\rho)$, the dynamical content of the background contributions is much less understood, e.g., in terms of Regge exchanges or coherent contributions from competing processes leading to $\pi^+\pi^-p$ final state.^{25,26}

We conclude that the determination of the ρ^0 resonance parameters from production cross-section data alone is difficult not only because the ρ^0 resonance is not narrow (see "Note on the ρ^0 mass and width" in Ref. 27). The averaging over the spin amplitudes introduces additional uncertainties which are process dependent and vary with s and t .

VI. SUMMARY

In a single experiment with a transversely polarized neutron target we measured reaction $\pi^+n \rightarrow \pi^+\pi^-p$ and determined average values of 14 spin-density-matrix elements in small (t,m) bins at 5.98 and 11.85 GeV/ c incident momentum. The measurement investigated the region $-t=0.1-1.0$ (GeV/ c)² and $m=0.36-1.04$ GeV. Possible D -wave contribution was found to be small with the exceptions described in Sec. IV B. The three spin-density-matrix elements which determine the relative phases between the natural and unnatural exchange amplitudes of the same transversity were obtained with large statistical errors due to the geometry of the apparatus.

Equations (5.5) and (5.7) relate the measured observables to linear combinations of moduli squared of recoil transversity amplitudes. We used them to construct bounds on the moduli of the P -wave amplitudes. The basic features of these bounds are necessarily common to the two solutions obtained in a more detailed amplitude analysis presented in Ref. 13.

Our results on the t dependence in the ρ^0 mass range show that, in contrast to the region of very small t , the contributions to the $\pi^+\pi^-$ production other than π exchange are rapidly becoming comparable to the π -exchange contribution and even larger as $|t|$ increases. We find clear evidence for A_1 exchange in all S - and P -wave nucleon helicity-nonflip amplitudes. The natural-

spin-parity A_2 -exchange amplitudes dominate at $-t \geq 0.5$ (GeV/ c)². The crossover of $|N|^2$ and $|\bar{N}|^2$ at $-t \simeq 0.45$ (GeV/ c)² is also seen in A_2 -exchange amplitudes at 6 GeV/ c in an amplitude analysis of SU(3)-related reactions.²³

Our study of the mass dependence in the region $-t=0.2-0.4$ (GeV/ c)² provides new and interesting information. In general, the unnatural exchange amplitudes with transversity down are larger than those with transversity up. The opposite is true for the natural exchange amplitudes. All P -wave transversity-up amplitudes show a peak at the ρ^0 mass. The s -channel transversity-down amplitudes for the dipion helicities $m = \pm 1$ show a clear dip at the ρ^0 mass. In terms of the nucleon-helicity-nonflip and -flip amplitudes A_n , $n=0,1$, our data on mass dependence confirm the presence of A_1 -exchange amplitudes. The amplitude U_0 is particularly large. The amplitude L_0 is small or close in phase to L_1 . The data also show that the relative phases $\Phi = \Phi_0 - \Phi_1$ are such that $\sin\Phi \leq 0$ for all amplitudes A_0 and A_1 , except at $m(\pi^+\pi^-) \leq 0.6$ GeV for the amplitudes U_0 and U_1 where $\sin\Phi > 0$.

In the range $-t=0.2-0.4$ (GeV/ c)² the resonance ρ^0 is produced by unnatural and natural exchanges, but in different spin-dependent manners. At the ρ^0 mass, the unnatural exchange amplitudes with transversities up and down contribute in equal amounts, while the production by natural exchange proceeds entirely with transversity up. The rapid changes of moduli of RTA for dipion helicities $m = \pm 1$ (U and N) near the ρ^0 mass were not seen in previous experiments. They could be due to rapid changes of the relative phases $\Phi = \Phi_0 - \Phi_1$. Alternatively, the amplitude U_0 could vanish and $|N_0| = |N_1|$ but 90° out of phase at the ρ^0 mass. We also observe variations in the width and apparent position of the ρ^0 peak in the P -wave amplitudes. This can be explained qualitatively by the width modulating effect of the pole residues and the interference with background terms, respectively. Variations in the apparent position and width of the ρ -mass peak had been observed previously in the reaction $\pi^+p \rightarrow \pi^+\pi^0p$ at lower energies and have been interpreted as interference with background from nucleon diffraction dissociation.²⁶

In this range of $-t$ from 0.2 to 0.4 (GeV/ c)² the upper bound for the S -wave contribution near the ρ^0 mass is of the order of 30% of the cross section. The mass dependence of the bounds on $|S|^2$ and $|\bar{S}|^2$ cannot exclude the possibility of an S -wave resonance in the region $m=0.7$ to 0.8 GeV (Ref. 28). A detailed discussion of this subject is presented in Ref. 13. We note that theoretical models concerning gluonic mesons (glueballs) seem to agree that the scalar state decaying into $\pi^+\pi^-$ should be the lightest state with a possible mass as low as 0.5 GeV (Ref. 29). The detailed experimental study of the S -wave is clearly of great interest.

The theoretical understanding of the mass dependence of the exchange mechanism in production processes has been scant due to the lack of data that can be obtained only in polarization experiments. Our results suggest that dedicated polarization experiments could be very rewarding in revealing new information.

The complete results of this experiment and the associated amplitude analysis¹³ are available on request in the form of numerical tables.¹⁴

Note added in proof. A detailed study of the S -wave amplitudes in the amplitude analysis of $\pi N \rightarrow \pi^+ \pi^- N$ measurements on polarized targets at 6, 12, and 17.2 GeV/c revealed a new resonance with a mass of $\simeq 750$ MeV and width $\simeq 100$ MeV. This 0^{++} (750) meson is

best understood as the lowest-mass 0^{++} (gg) gluonium state.^{30,31}

ACKNOWLEDGMENTS

This work was supported by Commissariat à l'Énergie Atomique, Saclay, France and, in part, by Fonds Formation de Chercheurs et Action Concertée (FCAC), Ministère de l'Éducation du Québec, Canada.

*Permanent address: Dawson College and McGill University, Montreal, Canada.

† Present address: GIXI Ingénierie et Informatique, Paris, France.

‡ Present address: AEI Industries, Tokyo, Japan.

§ Present address: Los Alamos Scientific Laboratory, Los Alamos, NM 87545.

** Present address: KEK, National Laboratory for High Energy Physics, Tsukuba, Japan.

¹M. Babou *et al.*, Nucl. Instrum. Methods. **160**, 1 (1979).

²M. Fujisaki *et al.*, Phys. Lett. **80B**, 314 (1979).

³M. Fujisaki *et al.*, Nucl. Phys. **B151**, 206 (1979).

⁴H. A. Gordon *et al.*, Phys. Rev. D **8**, 779 (1973).

⁵A. B. Wicklund *et al.*, Phys. Ref. D **17**, 1197 (1978).

⁶H. Becker *et al.*, Nucl. Phys. **B150**, 301 (1979); Nucl. Phys. **B151**, 46 (1979).

⁷B. R. Martin, D. Morgan, and G. Shaw, *Pion-Pion Interactions in Particle Physics* (Academic, New York, 1976); J. L. Petersen, *Pion-Pion Scattering* (CERN Yellow Report No. 77-04); C. B. Lang, Fortschr. Phys. **26**, 509 (1980).

⁸A. C. Irving and R. P. Worden, Phys. Rep. **34**, 119 (1977); C. Bourrely, E. Leader, and J. Soffer, *ibid.* **59**, 95 (1980).

⁹P. Hoyer and J. Kwiecinski, Nucl. Phys. **B60**, 26 (1973); P. Hoyer, P. Eastabrooks, and A. D. Martin, Phys. Rev. D **10**, 80 (1974).

¹⁰J. D. Kimel and J. F. Owens, Nucl. Phys. **B122**, 464 (1977).

¹¹G. Lutz and K. Rybicky, Internal Report, Munich, No. MPI-PAE/Exp. El. **75**, 1978 (unpublished).

¹²A. de Lesquen *et al.*, in *Low and Intermediate Energy Kaon-Nucleon Physics*, proceedings of the Workshop, Rome, 1980, edited by E. Ferrari and G. Violini (D. Reidel, Dordrecht, 1981), p. 289; M. Svec *et al.*, *ibid.*, p. 305; A. Itano *et al.*, in *High Energy Physics with Polarized Beams and Targets*, proceedings of the 1980 International Symposium, Lausanne, edited by C. Joseph and J. Soffer (Birkhauser, Boston, 1981), p. 560; M. Svec *et al.*, *ibid.* p. 566.

¹³M. Svec, A. de Lesquen, and L. van Rossum (unpublished).

¹⁴A. de Lesquen *et al.*, Saclay Internal Report DPhPE No. 82-01, 1982 (unpublished).

¹⁵D. Kemp *et al.*, Nuovo Cimento **27**, 155 (1975).

¹⁶R. V. Reid, Jr., Ann. Phys. (N.Y.) **50**, 411 (1968).

¹⁷A. Boudard, Département de Physique Nucléaire de Moyennes Energies, CEN Saclay (private communication).

¹⁸W. T. Eadie *et al.*, *Statistical Methods in Experimental Physics* (North-Holland, Amsterdam, 1971).

¹⁹G. Grayer *et al.*, Nucl. Phys. **B75**, 189 (1979).

²⁰P. La France and P. Winternitz, Phys. Rev. D **27**, 112 (1983).

²¹Ph. E. Gill, W. Murray, and M. H. Wright, *Practical Optimization* (Academic, New York, 1981).

²²P. Bonamy *et al.*, Nucl. Phys. **B52**, 392 (1973); O. Guisan *et al.*, Phys. Lett. **18**, 200 (1965).

²³M. Fujisaki *et al.*, Nucl. Phys. **B152**, 232 (1979).

²⁴G. Girardi *et al.*, Nucl. Phys. **B76**, 541 (1974); G. Girardi and H. Navelet, *ibid.* **B83**, 377 (1974).

²⁵E. Byckling and K. Kajantie, *Particle Kinematics* (Wiley, New York, 1973), pp. 115 and 257.

²⁶W. Michael, Phys. Rev. D **7**, 1985 (1973); J. MacNaughton *et al.*, Nucl. Phys. **B108**, 75 (1976).

²⁷Particle Data Group, R. L. Kelly *et al.*, Rev. Mod. Phys. **52**, S117 (1980); M. Roos *et al.*, Phys. Lett. **111B**, 122 (1982).

²⁸P. Estabrooks *et al.*, in π - π Scattering—1973, proceedings of the International Conference, Tallahassee, edited by D. K. Williams and W. Hagopian (AIP), New York, 1973, p. 37; J. T. Donohue and Y. Leroyer, Nucl. Phys. **B158**, 123 (1979); N. M. Cason *et al.*, Phys. Rev. D **28**, 1586 (1983).

²⁹R. Zitoun, in *Workshop on SPS Fixed Target Physics in the Years 1984–89*, edited by I. Mannelli (Report No. CERN 83-02), Vol. II, p. 338.

³⁰M. Svec, contributed paper to XXII International Conference on High Energy Physics, Leipzig, 1984 (unpublished).

³¹M. Svec, in *Proceedings of the 6th International Symposium on High Energy Spin Physics, Marseille, 1984*, edited by J. Soffer [J. Phys. (Paris) Colloq. **46**, C2-281 (1985)].